# Evaluation of Electronic Interaction Matrix Elements for Photoinduced Electron Transfer Processes within Mixed-Valence Complexes

**Bobak Gholamkhass, Koichi Nozaki,* and Takeshi Ohno**

*Department of Chemistry, Graduate School of Science, Osaka University, 1-16 Machikaneyama, Toyonaka, 560 Japan*

*Received: April 10, 1997; In Final Form: August 3, 1997*[⊗]

The photochemical properties of "alkane-bridged" binuclear complexes, $[(bec)_2Ru^{II}(L\text{-}C_n\text{-}L)Ru^{II/III}(bpy)_2]^{4+/5+}$ (where bec = 4,4′-bis(ethoxycarbonyl)-2,2′-bipyridine, bpy = 2,2′-bipyridine, and $n$ = 3, 4, 5, 10) and $[(dmb)_2Ru^{II}(L\text{-}C_n\text{-}L)Os^{II/III}(L_\alpha)_2]^{4+/5+}$ (where dmb = 4,4′-dimethyl-2,2′-bipyridine, $L_\alpha$ = bpy or dmb and $n$ = 3, 4, 5), in which the bridging ligand (L-$C_n$-L) was made of two [2-(2-pyridyl)-1-benzimidazolyl] groups (L) linked by an alkane chain, have been investigated using time-resolved nano- and picosecond laser spectroscopy. In the Ru(II)−Os(II) binuclear complexes, a metal-to-ligand charge transfer (MLCT) state of the Ru(II) moiety, ($^3$CT)Ru, was quenched by ($^3$CT)Ru → Os(II) energy transfer. The intramolecular energy transfer rates for $n$ = 3, 4, and 5 are well understood by assuming the Förster-type mechanism provided that the methylene chains are in a nearly extended form. In the mixed-valence binuclear complexes, Ru(II)−M(III) (M = Ru or Os), the decay of the ($^3$CT)Ru excited state was accelerated by electron transfer (ET) to the adjacent M(III) site giving the valence-isomer state, Ru(III)−M(II), which decayed to the ground state of the original form via back ET. Forward ET rates ($k_{et}$) have been determined from the decay rate of the ($^3$CT)Ru excited state ($k_{es}$) and the production yields of Ru(III)−M(II), $\phi_{et}$, and back ET rates ($k_b$) were obtained from the decay of Ru(III)−M(II). The value of $\phi_{et}$ ($\leq 0.5 \pm 0.1$) decreases along with the decreasing number of methylene groups or temperature, indicating the existence of another process quenching the ($^3$CT)Ru excited state. From the temperature dependence of $k_{et}$ and $k_b$, the electronic interaction matrix elements ($H_{rp}$) have been estimated using a nonadiabatic ET theory. $H_{rp}$ for the forward ET process was found to be enhanced by a factor of 2 in the compounds in which the excited electron locates on the bridging ligand in $[(dmb)_2Ru^{II}\text{-}(L\text{-}C_n\text{-}L)Os^{III}(L_\alpha)_2]^{5+}$ compared to that for $[(bec)_2Ru^{II}(L\text{-}C_n\text{-}L)Ru^{III}(bpy)_2]^{5+}$ ($n$ = 4, 5) in which the electron locates on the remote ligands. On the other hand, the matrix elements for back ET were found to be the same in either case, independent of metal ions and remote ligands.

## Introduction

Mixed-valence (MV) compounds have been studied to understand electron transfer (ET) process from several points of view. Those studies have provided information on the various important parameters that control ET rates. For example, reorganization energy ($\lambda$) and extent of electronic interaction matrix element ($H_{rp}$) for ET in MV compounds are estimated by analyzing a metal-to-metal charge transfer (MMCT) band of MV compounds in cases where this band is observable.[1,2]

Rates of ET in symmetrical MV complexes (self-exchange process, eq 1) have been determined from the line width in the magnetic resonance spectra.[3,4]

$$M_1(II)-M_1(III) \leftrightarrow M_1(III)-M_1(II) \qquad \text{"self-exchange ET"} \quad (1)$$

Effects of the solvent[3] or pressure[4] on the self-exchange ET rates have been studied. As for strongly coupled unsymmetric MV complexes, $[M_1(II)-M_2(III)]$, formation of the thermally unstable valence-isomer state, $[M_1(III)-M_2(II)]$, is followed by back electron transfer (BET) on the excitation of the MMCT bands (eqs 2 and 4).

$$M_1(II)-M_2(III) \rightarrow M_1(III)-M_2(II) \qquad \text{"MMCT"} \quad (2)$$

$$M_1(II)-M_2(III) \rightarrow {}^*M_1(II)-M_2(III) \rightarrow M_1(III)-M_2(II) \quad (3)$$

$$M_1(III)-M_2(II) \rightarrow M_1(II)-M_2(III) \qquad \text{"BET"} \quad (4)$$

Ultrafast solvation dynamics on BET following MMCT-band excitation was studied for CN-bridged Fe(II)−Fe(III)[5a] or Ru(II)−Fe(III)[5b] MV complexes by means of femtosecond laser kinetic spectroscopy. In weakly coupled MV compounds of which the MMCT band is too weak to be excited, it is occasionally possible to observe ET from an excited metal moiety to the other metal moiety and succeeding BET (eqs 3 and 4).[6,7] In the previous report, we have found that the valence-isomer state was formed when a Ru(II)−Ru(III) complex was excited into the ($^3$CT)Ru(II)−Ru(III) state (eq 3).[6a] However, it was found that the isomer state was not efficiently observed, suggesting the presence of a rapid quenching process, namely, energy transfer.[6a] In addition, since less information can be spectroscopically obtained from the weak MMCT band, the determination of $H_{rp}$ and $\lambda$ for these ET processes requires elaborate treatment of the rates using adequate assumptions. Also, the quenching rate of the metal-to-ligand charge-transfer (MLCT) excited state of the Ru(II), ($^3$CT)Ru, is not always equal to that of ET. Therefore, accurate forward ET rates can be exclusively estimated on the basis of not only the quenching rates but also quantitative analysis of ET products.

* To whom correspondence should be addressed. Fax: 0081-6-850-5785. E-mail: Nozaki@ch.wani.osaka-u.ac.jp.

[⊗] Abstract published in *Advance ACS Abstracts,* October 1, 1997.

S1089-5647(97)01240-6 CCC: $14.00 © 1997 American Chemical Society

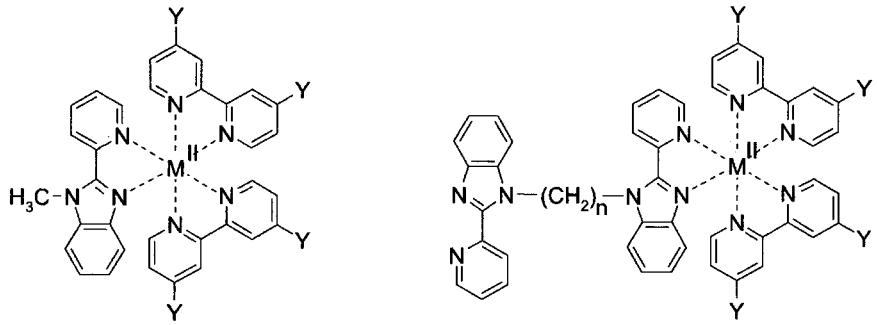

Y=H, M= Ru : $[(bpy)_2Ru(mpbim)]^{2+}$ , $[(bpy)_2Ru(L\text{-}C_n\text{-}L)]^{2+}$
Y=$CH_3$, M= Ru : $[(dmb)_2Ru(mpbim)]^{2+}$ , $[(dmb)_2Ru(L\text{-}C_n\text{-}L)]^{2+}$ , n = 3, 4, 5
Y=OCOEt, M= Ru : $[(bec)_2Ru(mpbim)]^{2+}$ , $[(bec)_2Ru(L\text{-}C_n\text{-}L)]^{2+}$, n = 3, 4, 5, 10
Y=H, M= Os : $[(bpy)_2Os(mpbim)]^{2+}$ , $[(bpy)_2Os(L\text{-}C_n\text{-}L)]^{2+}$
Y=$CH_3$, M= Os : $[(dmb)_2Os(mpbim)]^{2+}$ , $[(dmb)_2Os(L\text{-}C_n\text{-}L)]^{2+}$, n =3, 4, 5

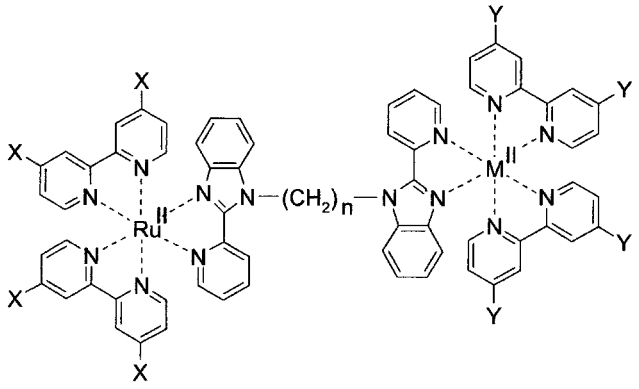

M= Os, X= $CH_3$, Y= H, n= 3, 4, 5 : $[(dmb)_2Ru(L\text{-}C_n\text{-}L)Os(bpy)_2]^{4+}$
M= Os, X= $CH_3$, Y= $CH_3$, n= 4, 5 : $[(dmb)_2Ru(L\text{-}C_n\text{-}L)Os(dmb)_2]^{4+}$
M= Ru, X= OCOEt, Y= H, n= 3, 4, 5, 10 : $[(bec)_2Ru(L\text{-}C_n\text{-}L)Ru(bpy)_2]^{4+}$

**Figure 1.** Structural formulas of the mono- and binuclear complexes. The abbreviations used in this paper are also shown.

When the ET occurs from the ($^3$CT)Ru state to the electron acceptor linked with a certain bridging ligand, the most important feature when interpreting the photoinduced ET process is that the ET rate depends on whether the excited electron locates on the nonbridging ligand or the bridging one. Elliott *et al.* have clarified these phenomena through the interpretation of the photoinduced ET rates in Ru(II)−$DQ^{2+}$ with a variation of the nonbridging ligands.[8] The rates were well interpreted by assuming that (1) the ET occurs only from the bridging ligand and (2) the excited electron distributes between the bridging and nonbridging ligands depending on the difference between the energy levels of their LUMO. Although the validity of this assumption depends on the difference between the ET rates from the nonbridging ligands and the bridging ligand, a comparison between these ET rates has not been made so far.

Compounds examined in this work are Ru(II)−Ru(III) and Ru(II)−Os(III) MV complexes shown in Figure 1. We report here the production yield of the valence-isomer state ($\phi_{et}$), the forward ET rates, and the BET rates in those compounds. The variations in ET rates with remote ligands or the number of methylene groups are discussed on the basis of ET parameters, $H_{rp}$ and $\lambda$, which are determined by analyzing the temperature dependence of the forward and backward ET rates using a nonadiabatic ET theory.

## Experimental Section

**Materials.** Acetonitrile (AN) was purified by distillation over $P_2O_5$. Butyronitrile (BN) was distilled over $P_2O_5$ under a reduced pressure. All other chemicals were of analytical grade and used as supplied.

**Preparation.** The preparation of tetradentate bridging ligands (L-$C_n$-L), 1,3-bis[2-(2-pyridyl)-1-benzimidazolyl]propane (L-$C_3$-L), 1,4-bis[2-(2-pyridyl)-1-benzimidazolyl]butane (L-$C_4$-L), 1,5-bis[2-(2-pyridyl)-1-benzimidazolyl]pentane (L-$C_5$-L) and 1,10-bis[2-(2-pyridyl)-1-benzimidazolyl]decane (L-$C_{10}$-L) were reported previously.[9] The mononuclear complexes, $[(bpy)_2Ru(mpbim)](ClO_4)_2$ (mpbim = *N*-methyl-2-(2-pyridyl)benzimidazole), $[(bpy)_2Ru(L\text{-}C_5\text{-}L)](ClO_4)_2$, $[(dmb)_2Ru(L\text{-}C_5\text{-}L)](ClO_4)_2$, and $[(bec)_2Ru(L\text{-}C_5\text{-}L)](ClO_4)_2$, and the binuclear complexes, $[(dmb)_2Ru(L\text{-}C_5\text{-}L)Ru(dmb)_2](ClO_4)_4$ and $[(bpy)_2Ru(L\text{-}C_5\text{-}L)Ru(bec)_2](PF_6)_4$, were described elsewhere.[9]

*Os(II) Complexes. (a) $[Os(bpy)_2(L\text{-}C_5\text{-}L)](ClO_4)_2$.* $Os(bpy)_2Br_2$ (100 mg) and L-$C_5$-L (73.6 mg) in a mixture of ethanol and water (20 mL, 4:1 v/v) were refluxed for 30 h. The ethanol was then evaporated, and water was added. The unreacted ligand was extracted by toluene, and then a saturated solution of $NaClO_4$ was added. The resulting dark green precipitate was filtered and washed with 0.5 mL of cold distilled water. The crude product was chromatographically purified over a SP-Sephadex C-25 column using an acetonitrile-buffered water (pH = 4.7) mixture (1:1 v/v) as eluent. Further purification was achieved through recrystallization from a mixture of ethanol and water (2:3 v/v). Yield: 68 mg. Electrospray ionization mass spectra (ESI−MS):[10] $m/z$ = 481, $[M\text{-}2ClO_4^-]^{2+}$; 531, $[M\text{-}ClO_4^-]^{2+}$.

*(b) $[Os(dmb)_2(L\text{-}C_5\text{-}L)](PF_6)_2$.* The synthesis method of this

compound was the same as above except that a saturated solution of $NH_4PF_6$ was added to precipitate the product instead of a solution of $NaClO_4$. Yield: 53 mg. ESI-MS: $m/z = 509$, $[M\text{-}2PF_6^-]^{2+}$; 1163, $[M\text{-}PF_6^-]^+$.

*(c) [Os(bpy)$_2$(L-C$_4$-L)](PF$_6$)$_2$.* $Os(bpy)_2Br_2$ (50 mg) and L-$C_4$-L (35 mg) in 5 mL of ethylene glycol were stirred under an argon atmosphere for 5 min. The mixture was then refluxed for 15 min. After the solution cooled to room temperature, it was diluted with distilled water and an appropriate amount of a saturated $NH_4PF_6$ solution was added to precipitate the product. The resulting dark-green precipitate was purified as described for $[Os(bpy)_2(L\text{-}C_5\text{-}L)](ClO_4)_2$. Yield: 50 mg.

*(d) [Os(dmb)$_2$(L-C$_4$-L)](PF$_6$)$_2$.* The synthesis and purification method of this compound were same as that for $[Os(bpy)_2(L\text{-}C_4\text{-}L)](PF_6)_2$. Yield: 41 mg.

*(e) [Os(bpy)$_2$(L-C$_3$-L)](PF$_6$)$_2$.* The preparation and purification of this compound were analogous to that of $[Os(bpy)_2(L\text{-}C_4\text{-}L)](PF_6)_2$, using L-$C_3$-L instead of L-$C_4$-L. Yield: 47 mg.

*Ru(II)−Os(II) Complexes. (a) [(dmb)$_2$Ru(L-C$_5$-L)Os(bpy)$_2$](PF$_6$)$_4$.* $[Os(bpy)_2(L\text{-}C_5\text{-}L)](ClO_4)_2$ (20 mg) and $Ru(dmb)_2Cl_2$ (11 mg) in 20 mL of an ethanol−water mixture (4:1) were refluxed for 4 h. After the mixture cooled, the ethanol was evaporated and the product precipitated by addition of aqueous $NH_4PF_6$. The crude product was chromatographically purified over a CM-Sephadex C-25 column using an acetonitrile-buffered water (pH = 5.7) mixture (1:1 v/v) as eluent. The product was further purified by recrystallization from a mixture of ethanol and water. Yield: 22.7 mg. ESI-MS: $m/z = 525$, $[M\text{-}3PF_6^-]^{3+}$; 860, $[M\text{-}2PF_6^-]^{2+}$.

*(b) [(dmb)$_2$Ru(L-C$_5$-L)Os(dmb)$_2$](PF$_6$)$_4$.* This compound was synthesized from $[Os(dmb)_2(L\text{-}C_5\text{-}L)](ClO_4)_2$ (20 mg) and $Ru(dmb)_2Cl_2$ (10 mg) in the same manner as above. Yield: 16.5 mg. ESI-MS: $m/z = 544$, $[M\text{-}3PF_6^-]^{3+}$; 372, $[M\text{-}4PF_6^-]^{4+}$.

*(c) [(dmb)$_2$Ru(L-C$_4$-L)Os(bpy)$_2$](PF$_6$)$_4$.* A mixture of $[Os(bpy)_2(L\text{-}C_4\text{-}L)](PF_6)_2$ (15 mg) and $Ru(dmb)_2Cl_2$ (6.5 mg) in 5 mL of ethylene glycol was stirred with Ar purging for 5 min. The mixture was then refluxed for 10 min. After the mixture cooled to room temperature, a saturated $NH_4PF_6$ solution was added. The resulting dark-green precipitate was purified as for $[(dmb)_2Ru(L\text{-}C_5\text{-}L)Os(bpy)_2](PF_6)_4$. Yield: 20.5 mg. ESI-MS: $m/z = 521.6$, $[M\text{-}3PF_6^-]^{3+}$; 355, $[M\text{-}4PF_6^-]^{4+}$.

*(d) [(dmb)$_2$Ru(L-C$_4$-L)Os(dmb)$_2$](PF$_6$)$_4$.* The preparation method of this complex was analogous to that of $[(dmb)_2Ru(L\text{-}C_4\text{-}L)Os(bpy)_2](PF_6)_4$. Yield: 22 mg. ESI-MS: $m/z = 540$, $[M\text{-}3PF_6^-]^{3+}$; 369, $[M\text{-}4PF_6^-]^{4+}$.

*(e) [(dmb)$_2$Ru(L-C$_3$-L)Os(bpy)$_2$](PF$_6$)$_4$.* This compound was synthesized from $[Os(bpy)_2(L\text{-}C_3\text{-}L)](PF_6)_2$ (17 mg) and $Ru(dmb)_2Cl_2$ (7.8 mg) in the same manner as for $[(dmb)_2Ru(L\text{-}C_4\text{-}L)Os(bpy)_2](PF_6)_4$. Yield: 27.4 mg. ESI-MS: $m/z = 517$, $[M\text{-}3PF_6^-]^{3+}$; 352, $[M\text{-}4PF_6^-]^{4+}$.

**Measurements.** Absorption spectra were measured on a Hitachi spectrophotometer (U-3400). Emission spectra were recorded either with a spectrofluorometer (Hitachi MPF-4) or with an argon ion laser (Innova 300, $\lambda_{ex} = 488$ nm, Coherent) using a grating monochromator (Jasco CT250) with silicon diode array (Hamamatsu S3901-512Q).

The system of nanosecond kinetic spectroscopy was reported previously.[11] Picosecond time-resolved transient absorption spectra were obtained using a picosecond laser photolysis system with a mode-locked $Nd^{3+}$:YAG laser (Continuum PY61C-10).[12] The second harmonics (532 nm, 5 mJ pulse$^{-1}$, fwhm = 17 ps, 10 Hz) was used for the excitation of a solution of a binuclear complex in a 2 mm quartz cell. The measurement in a glassy BN solution was performed using a 0.2 mm cell. Transient emission with a lifetime less than 20 ns was measured using an avalanche PIN photodiode (Hamamatsu Photonics S2383) with the mode-locked $Nd^{3+}$:YAG laser excitation.[12]

Temperature of a sample solution was regulated from 130 to 300 K by using a cryostat (Oxford DN 1704) and a controller (Oxford ITC4).

Redox potentials of metal complexes were measured by differential-pulse voltammetry using a dc pulse polarograph (Huso, HECS-312B). Voltamograms were recorded using a platinum disk electrode (diameter 0.5 mm) in an AN solution of the complexes containing 0.1 M tetraethylammonium perchlorate (TEAP).

Electronic spectra of a mononuclear complex in an oxidized form were measured by means of the column-electrolysis reported previously.[11] An AN solution containing both ca. 0.5 mM of a Ru(II) complex and 0.1 M TEAP was passed through the column electrode fabricated by packing platinum wires (diameter 0.1 mm) in a porous glass tube (pore size 20 nm, inner diameter 2 mm, length 20 mm). The electrolyzed solution was then transferred to an optical cell (length 2 mm). The potential of the electrode was controlled using a homemade potentiostat. The efficiency of the electrolysis was more than 95%.

The difference molar absorption coefficients ($\Delta\epsilon$) of a $^3$CT excited state of a Ru(II) mononuclear complex were evaluated by assuming 100%-efficient energy transfer from ($^3$CT)Ru to anthracene.[13] The absorption coefficients obtained in an AN solution are as follows: $\Delta\epsilon(460\text{ nm}) = -9500\ M^{-1}\ cm^{-1}$ for $[Ru(bpy)_2mpbim]^{2+}$, $\Delta\epsilon(490\text{ nm}) = -10\,200\ M^{-1}\ cm^{-1}$, $\Delta\epsilon(532\text{ nm}) = -1000\ M^{-1}\ cm^{-1}$ for $[Ru(bec)_2(L\text{-}C_5\text{-}L)]^{2+}$, and $\Delta\epsilon(460\text{ nm}) = -7760\ M^{-1}\ cm^{-1}$ for $[Ru(bpy)_2(L\text{-}C_5\text{-}L)]^{2+}$.

## Results

**Absorption and Emission Spectra.** Absorption spectra of mononuclear complexes, $[(dmb)_2Ru(L\text{-}C_5\text{-}L)]^{m+}$, $[(L_\alpha)_2Os(L\text{-}C_5\text{-}L)]^{m+}$, $m = 2$, 3, and binuclear complexes, $[(dmb)_2Ru(L\text{-}C_5\text{-}L)Os(L_\alpha)_2]^{4+}$, $L_\alpha$ = bpy or dmb, are shown in parts a, b, and c of Figure 2, respectively. The absorption maxima of all the complexes are collected in Table 1. These complexes show bridging ligand-centered transition with $\epsilon \sim 1 \times 10^4\ M^{-1}\ cm^{-1}$ around 330 nm. For Ru(II) or Os(II) complexes, MLCT ($d\pi(t_{2g}) \rightarrow \pi^*(L)$) bands with $1 \times 10^4 < \epsilon < 2 \times 10^4\ M^{-1}\ cm^{-1}$ appeared in the range of 400−700 nm. A broad absorption band around 550 nm ($\epsilon = 1600\ M^{-1}\ cm^{-1}$) in Os(III) complexes is due to LMCT transition that occurs between ligand-$\pi$ orbital to $d\pi$ orbital of the Os(III) ion. In the case of Ru(III) complexes, the LMCT band appeared in a longer wavelength (around 650 nm, $\epsilon = 2200\ M^{-1}\ cm^{-1}$). The spectra of binuclear complexes were reproduced as the sum of the Ru(II) and Os(II) mononuclear components. In MV compounds, the intensity of intervalence transition (IT) band was too weak to be observed in the near IR region ($\epsilon < 100\ cm^{-1}$). These results indicate the absence of any strong electronic interaction between Ru(II) and Os(II) moieties.

The maxima and the lifetimes of emission for mononuclear complexes, $[(L_\alpha)_2M(L\text{-}C_5\text{-}L)]^{2+}$, M = Os(II), Ru(II), and for binuclear complexes, $[(dmb)_2Ru(L\text{-}C_n\text{-}L)Os(L_\alpha)_2]^{4+}$, $n = 3$, 4, 5; $L_\alpha$ = bpy, dmb, and bec, are presented in Table 2. The emission maxima were blue-shifted at 77 K compared with those at room temperature. The extent of the shift in the Os(II) complexes (0.6−1.0 kK) was less than that of the Ru(II) complexes (1.1−1.3 kK). The emission quantum yields in a BN solution of the mononuclear Ru(II) complexes were smaller than that of $[Ru(bpy)_3]^{2+}$.[14]

On comparing the emission of the binuclear complexes, $[(dmb)_2Ru(L\text{-}C_n\text{-}L)Os(L_\alpha)_2]^{4+}$, with that of an isoabsorbative

**TABLE 1: Absorption Maxima of Ru(II/III) and Os(II/III) Mononuclear and Ru(II)−Os(II) and Ru(II)−Ru(II) Binuclear Complexes[a]**

| | $\tilde{\nu}_{max}/10^3$ cm$^{-1}$ ($\epsilon_{max}$[b]/$10^3$ M$^{-1}$ cm$^{-1}$) | | | | | | | | |
|---|---|---|---|---|---|---|---|---|---|
| compound | $\pi-\pi^*$ | | MLCT | | | | d$\pi$−d$\pi$ | | |
| $[(bpy)_2Ru(L\text{-}C_5\text{-}L)]^{2+}$ | 34.6(89) | 32.3(51) | | 21.8(16.3) | | | | | |
| $[(bpy)_2Ru(L\text{-}C_5\text{-}L)]^{3+}$ | | | | | | | 14.7(2) | | |
| $[(dmb)_2Ru(L\text{-}C_3\text{-}L)]^{2+}$ | 34.8(76) | 32.7(49.6) | | 21.6(15.3) | | | | | |
| $[(dmb)_2Ru(L\text{-}C_3\text{-}L)]^{3+}$ | 33.1(57) | 32.2(58.7) | | | | | 15.5(1.7) | | |
| $[(dmb)_2Ru(L\text{-}C_5\text{-}L)]^{2+}$ | 34.6(75) | 32.3(47) | | 21.5(14.1) | | | | | |
| $[(dmb)_2Ru(L\text{-}C_5\text{-}L)]^{3+}$ | | | | | | | 15.2(2) | | |
| $[(bec)_2Ru(L\text{-}C_5\text{-}L)]^{2+}$ | 32.4(93) | 27.2(14.2) | 22.3(16.0) | 20.5(19.6) | | | | | |
| $[(bec)_2Ru(L\text{-}C_5\text{-}L)]^{3+}$ | | | | | | | 13.5(2.3) | | |
| $[(bpy)_2Os(L\text{-}C_3\text{-}L)]^{2+}$ | 34.2(79) | 32.3[c] | 22.1(11.2) | 20.5(12.5) | 16.5(3.2) | 15.2(3.0) | | | |
| $[(bpy)_2Os(L\text{-}C_3\text{-}L)]^{3+}$ | 32.8(47.6) | | | | | | 18.6(1.2) | 5.6(0.2) | 4.3(0.9) |
| $[(bpy)_2Os(L\text{-}C_4\text{-}L)]^{2+}$ | 34.2(85) | 32.3[c] | 22.0(12.5) | 20.6(13.8) | 16.6(3.5) | 15.2(3.2) | | | |
| $[(bpy)_2Os(L\text{-}C_4\text{-}L)]^{3+}$ | 32.9(48.5) | | | | | | 18.9(1.3) | 5.6(0.4) | 4.2(0.8) |
| $[(bpy)_2Os(L\text{-}C_5\text{-}L)]^{2+}$ | 34.1(89) | 31.7(40) | 22.0(12.0) | 20.2(13.5) | 16.4(3.8) | 14.9(3.5) | | | |
| $[(bpy)_2Os(L\text{-}C_5\text{-}L)]^{3+}$ | | | | | | | 18.2(1.6) | 5.4(0.2) | 4.3(0.7) |
| $[(dmb)_2Os(L\text{-}C_4\text{-}L)]^{2+}$ | 34.4(83) | 32.4[c] | 21.8(12.7) | 20.2(14.5) | 16.2(4.1) | 15.0(4.0) | | | |
| $[(dmb)_2Os(L\text{-}C_4\text{-}L)]^{3+}$ | | | | | | | 16.6(1.2) | 5.6(0.5) | 4.3(1) |
| $[(dmb)_2Os(L\text{-}C_5\text{-}L)]^{2+}$ | 34.2(82) | 31.7(40) | 22.0(11.5) | 20.2(12.4) | 16.4(3.5) | 14.9(3.2) | | | |
| $[(dmb)_2Os(L\text{-}C_5\text{-}L)]^{3+}$ | | | | | | | 17.4(1.6) | 5.3(0.3) | 4.3(0.6) |
| $[(bpy)_2Os(mpbim)]^{2+}$ | 34.2(82) | 31.1(28.7) | 22.0(14.9) | 20.5(16.3) | 16.6(4.2) | 15.0(3.9) | | | |
| $[(bpy)_2Os(mpbim)]^{3+}$ | | | | | | | 18.2(1.6) | 5.6(0.3) | 4.3(0.7) |
| $[(dmb)_2Ru(L\text{-}C_3\text{-}L)Os(bpy)_2]^{4+}$ | 34.5(125) | 31.4(39.0) | | 21.3(25.3) | 16.6(3.6) | 15.0(3.4) | | | |
| $[(dmb)_2Ru(L\text{-}C_4\text{-}L)Os(bpy)_2]^{4+}$ | 34.5(133) | 31.3(41.7) | | 21.4(27.4) | 16.5(3.9) | 15.2(3.7) | | | |
| $[(dmb)_2Ru(L\text{-}C_4\text{-}L)Os(dmb)_2]^{4+}$ | 34.6(129) | 31.7(43.0) | | 21.5(27.6) | 16.4(4.0) | 15.0(3.8) | | | |
| $[(dmb)_2Ru(L\text{-}C_5\text{-}L)Os(bpy)_2]^{4+}$ | 34.6(121) | 31.3(46.7) | | 21.5(26.0) | 16.5(3.5) | 15.0(3.2) | | | |
| $[(dmb)_2Ru(L\text{-}C_5\text{-}L)Os(dmb)_2]^{4+}$ | 34.6(130) | 31.3(52.9) | | 21.6(28.6) | 16.5(4.3) | 15.2(4.0) | | | |
| $[(bec)_2Ru(L\text{-}C_5\text{-}L)Ru(bpy)_2]^{4+}$ | 34.6(93.0) | 32.5(96.7) | | 21.8(30.0) | | | | | |

[a] All the spectra are obtained in an AN solution containing 0.05 M of TEAP at room temperature. [b] Estimated error in $\epsilon_{max}$ is ±5%. [c] Observed as a shoulder of the main band at ca. 34 500 cm$^{-1}$.

**TABLE 2: Emission Maxima ($\tilde{\nu}_{max}$), Lifetimes ($\tau$), and Emission Quantum Yield ($\phi_{em}$)[a]**

| | $\tilde{\nu}_{max}/10^3$cm$^{-1}$ ($\tau$/ns) | | | | | |
|---|---|---|---|---|---|---|
| | Os-moiety | | Ru-moiety | | | |
| compound | 298 K | 77 K | 298 K | $\phi_{em}$ | 77 K | $\phi_{em}$ |
| $[(bec)_2Ru(L\text{-}C_5\text{-}L)]^{2+}$ | | | 14.3(600 ± 10) | 0.016[b] | 15.4 | |
| $[(bpy)_2Ru(L\text{-}C_5\text{-}L)]^{2+}$ | | | 15.2(660 ± 10) | | 16.5(4760 ± 50) | |
| $[(dmb)_2Ru(L\text{-}C_5\text{-}L)]^{2+}$ | | | 14.8(700 ± 10) | 0.029[b] | 16.1(4060 ± 50) | 0.186[b] |
| $[(bpy)_2Os(mpbim)]^{2+}$ | 13.0 | 13.6 | | | | |
| $[(bpy)_2Os(L\text{-}C_5\text{-}L)]^{2+}$ | 12.9(34 ± 2) | 13.6 | | | | |
| $[(dmb)_2Os(L\text{-}C_5\text{-}L)]^{2+}$ | 12.3(32 ± 2) | 13.3 | | | | |
| $[(dmb)_2Ru(L\text{-}C_3\text{-}L)Os(bpy)_2]^{4+}$ | 12.9(39 ± 2) | 13.6 | 14.9(2.1 ± 0.2) | | 16.1(3.0 ± 0.2) | |
| $[(dmb)_2Ru(L\text{-}C_4\text{-}L)Os(bpy)_2]^{4+}$ | 12.9(33 ± 2) | 13.6(530 ± 20) | 14.9(3.6 ± 0.4) | | 16.1[c](5.1 ± 0.7) | |
| $[(dmb)_2Ru(L\text{-}C_5\text{-}L)Os(bpy)_2]^{4+}$ | 12.9(31 ± 2) | 13.6(525 ± 50) | 14.8(5.9 ± 1.0) | | 16.0(7.4 ± 0.2) | |
| $[(dmb)_2Ru(L\text{-}C_4\text{-}L)Os(dmb)_2]^{4+}$ | 12.3(29 ± 2) | 13.3(450 ± 15) | 14.9(2.8 ± 0.3) | | 16.1(4.8 ± 0.7) | |
| $[(dmb)_2Ru(L\text{-}C_5\text{-}L)Os(dmb)_2]^{4+}$ | 12.3(29 ± 2) | 13.3(455 ± 25) | 14.8(4.5 ± 1.0) | | 16.0(6.3 ± 0.9) | |

[a] Room-temperature luminescence spectra were obtained in AN and BN solutions were used for low temperature measurement. Emission maxima and lifetimes were measured with excitation at 488 and 532 nm, respectively. [b] Obtained in MeOH/EtOH (1:4) using $[Ru(bpy)_3]^{2+}$ as reference ($\phi_{em}$ = 0.073 at *RT* and $\phi_{em}$ = 0.376 at 77 K).[22b] [c] The emission of the Ru moiety was almost covered by tail emission of the Os moiety.

solution containing the equimolar parent mononuclear complexes, $[(dmb)_2Ru(L\text{-}C_n\text{-}L)]^{2+}$ and $[(L_\alpha)_2Os(L\text{-}C_n\text{-}L)]^{2+}$, the emission intensity from the Os(II) chromophore was enhanced while that from the Ru(II) site decreased. This result can be interpreted in terms of an intramolecular energy transfer process from ($^3$CT)Ru(II) to Os(II) moieties. The energy transfer rates were determined from the lifetimes of ($^3$CT)Ru in the binuclear complexes compared to those of $[(dmb)_2Ru(L\text{-}C_n\text{-}L)]^{2+}$ both at room temperature and 77 K. These rates were dependent on the number of methylene groups and slightly on temperature. Rates are collected in Table 3.

**TABLE 3: Energy Transfer Rates in Binuclear Complexes ($k_{EN}/10^8$ s$^{-1}$)[a]**

| | 298 K | | 77 K | |
|---|---|---|---|---|
| compound | obsd | calcd | obsd | calcd |
| $[(bpy)_2Os(L\text{-}C_3\text{-}L)Ru(dmb)_2]^{4+}$ | 4.7 ± 0.2 | 4.2 | 3.3 ± 0.2 | |
| $[(bpy)_2Os(L\text{-}C_4\text{-}L)Ru(dmb)_2]^{4+}$ | 2.7 ± 0.2 | 1.9 | 1.9 ± 0.2 | |
| $[(dmb)_2Os(L\text{-}C_4\text{-}L)Ru(dmb)_2]^{4+}$ | 3.6 ± 0.2 | 1.5 | 2.1 ± 0.3 | |
| $[(bpy)_2Os(L\text{-}C_5\text{-}L)Ru(dmb)_2]^{4+}$ | 1.7 ± 0.4 | 1.0 | 1.4 ± 0.1 | 1.0 |
| $[(dmb)_2Os(L\text{-}C_5\text{-}L)Ru(dmb)_2]^{4+}$ | 2.3 ± 0.5 | 0.8 | 1.6 ± 0.3 | 0.9 |
| $[(bpy)_2Ru(L\text{-}C_5\text{-}L)Ru(bec)_2]^{4+}$ | 0.13[b] | | 0.029[b] | 0.04[b] |

[a] Energy transfer rates were calculated assuming the Förster mechanism. [b] Reference 9.

**Redox Potentials.** Redox potentials of the ruthenium and the osmium complexes are presented in Table 4. The mononuclear complexes exhibited a reversible one-electron redox process corresponding to an M(III/II) couple. For all the binuclear complexes, the oxidation process of the Os(II) center followed by that of the Ru(II) center was observed on increasing the anodic potential. The metal-based redox potentials in binuclear complexes were similar to those of their monomeric parents (within ±25 mV).

**TABLE 4: Redox Potential of Mono- and Binuclear Ru(II) and Os(II) Complexes[a]**

| compound | $E°$/mV | | | | | | |
|---|---|---|---|---|---|---|---|
| $[(bpy)_2Ru(L\text{-}C_3\text{-}L)]^{2+}$ | | +780 | −1745 | −1935 | −2180 | | |
| $[(bpy)_2Ru(L\text{-}C_5\text{-}L)]^{2+}$ | | +765 | −1745 | −1935 | −2190 | | |
| $[(dmb)_2Ru(L\text{-}C_5\text{-}L)]^{2+}$ | | +655 | −1805 | −2030 | | | |
| $[(bec)_2Ru(L\text{-}C_5\text{-}L)]^{2+}$ | | +970 | −1340 | −1540 | −1700 | −1970 | |
| $[Ru(bpy)_3]^{2+}$ | | +875 | −1735 | −1925 | −2170 | | |
| $[Ru(dmb)_3]^{2+}$ | | +740 | −1915 | −2185 | −2520 | | |
| $[(bpy)_2Os(L\text{-}C_3\text{-}L)]^{2+}$ | +350 | | −1665 | −1860 | −2185 | | |
| $[(bpy)_2Os(L\text{-}C_4\text{-}L)]^{2+}$ | +350 | | −1665 | −1870 | −2210 | | |
| $[(bpy)_2Os(L\text{-}C_5\text{-}L)]^{2+}$ | +340 | | −1670 | −1865 | | | |
| $[(dmb)_2Os(L\text{-}C_4\text{-}L)]^{2+}$ | +250 | | −1730 | −1950 | | | |
| $[(dmb)_2Os(L\text{-}C_5\text{-}L)]^{2+}$ | +235 | | −1740 | −1965 | | | |
| $[Os(bpy)_3]^{2+}$ | +440 | | −1645 | −1845 | | | |
| $[(bpy)_2Os(mpbim)]^{2+}$ | +335 | | −1680 | −1885 | | | |
| $[(bpy)_2Os(L\text{-}C_3\text{-}L)Ru(dmb)_2]^{4+}$ | +340 | +655 | −1665 | −1800 | −1835 | −2025 | |
| $[(bpy)_2Os(L\text{-}C_4\text{-}L)Ru(dmb)_2]^{4+}$ | +345 | +660 | −1670 | −1820 | −1850 | | |
| $[(dmb)_2Os(L\text{-}C_4\text{-}L)Ru(dmb)_2]^{4+}$ | +245 | +660 | −1735 | −1780 | −2025 | | |
| $[(bpy)_2Os(L\text{-}C_5\text{-}L)Ru(dmb)_2]^{4+}$ | +340 | +655 | −1665 | −1850 | −2005 | | |
| $[(dmb)_2Os(L\text{-}C_5\text{-}L)Ru(dmb)_2]^{4+}$ | +235 | +650 | −1790 | −2010 | | | |
| $[(bpy)_2Ru(L\text{-}C_5\text{-}L)Ru(bec)_2]^{4+}$ | +755 | +945 | −1350 | −1540 | −1755 | −1955 | −2190 |

[a] At room temperature, in AN solutions containing 0.1 M of TEAP. All $E°$ values are referred to $E°$ of the ferrocenium$^+$/ferrocene redox couple ($E° = 0.36$ V vs SSCE in AN).

On reduction of these complexes, several redox processes have been observed between −1.3 and −2.5 V and were ascribed to the reduction of ligands.[15] The first reduction in mononuclear compounds, $[M(bpy)_3]^{2+}$ and $[(bpy)_2M(L\text{-}C_5\text{-}L)]^{2+}$ (M = Os and Ru), takes place on the bpy, whereas reduction of L-$C_5$-L is preferred in $[(dmb)_2M(L\text{-}C_5\text{-}L)]^{2+}$ because reduction occurred at ca. 100 mV less negative potential than for $[M(dmb)_3]^{2+}$. Furthermore, large positive shift (ca. 450 mV) of the first reduction potential in mono- and binuclear complexes consisting of bec indicates that the first reduction happens on the bec ligand. All the reduction potentials were shifted to less negative values by ca. 70 mV on replacing Ru(II) with Os(II) ion.

**Transient Absorption Spectra of Mononuclear Complexes.** Transient absorption (TA) spectra for the $^3$CT state of $[(L_\alpha)_2Ru(L\text{-}C_5\text{-}L)]^{2+}$, $L_\alpha$ = bpy, dmb, and bec, are shown in parts a, b, and c of Figure 3, respectively. In all the spectra, bleaching of the MLCT band was observed around 460−490 nm. For $[(dmb)_2Ru(L\text{-}C_5\text{-}L)]^{2+}$, two bands around 380 and 550 nm and one bleaching at 320 nm are representative of the formation of an L-$C_5$-L anion radical. Thus, the excited electron was found to be located on the bridging ligand. On the other hand, when $L_\alpha$ is bec, no band was observed around 550 nm and the other one appeared in the range of 330−380 nm. Together with this fact, the bleaching of $\pi-\pi^*$ transition of bec at 310 nm shows the preferred location of excited electron on bec rather than on the bridging ligand (L-$C_5$-L).

The TA spectrum for $[(bpy)_2Ru(L\text{-}C_5\text{-}L)]^{2+}$ was almost the same as for $[(dmb)_2Ru(L\text{-}C_5\text{-}L)]^{2+}$ except that the bleaching intensity at 320 nm was one-half of that of MLCT at 460 nm while the bleaching intensity at these two wavelengths are almost equal for $L_\alpha$ = dmb. At low temperature (163 K), the bleaching of $\pi-\pi^*$ band for bpy around 300 nm increased while the bleaching at 320 nm decreased in $[(bpy)_2Ru(L\text{-}C_5\text{-}L)]^{2+}$. Therefore, these results reveal that the energy of the $[(bpy)(bpy^-)Ru^{III}(L\text{-}C_5\text{-}L)]^{2+}$ state is slightly lower than that of $[(bpy)_2Ru^{III}(L^-\text{-}C_5\text{-}L)]^{2+}$, and the energy difference is comparable to the thermal energy at room temperature (∼25 meV). In the case of $[(dmb)_2Ru(L\text{-}C_5\text{-}L)]^{2+}$, no change in TA was observed on lowering the temperature from 298 to 163 K, indicating that the excited electron preferably localizes on the L-$C_5$-L in the temperature range of 163−300 K. At lower temperatures no change in the TA spectrum of $[(bec)_2Ru(L\text{-}C_5\text{-}L)]^{2+}$ was observed except sharpening of the MLCT band. Thus, the energy level of the $[(bec)(bec^-)Ru^{III}(L\text{-}C_5\text{-}L)]^{2+}$ state is lower by at least 50 meV than that of $[(bec)_2Ru^{III}(L^-\text{-}C_5\text{-}L)]^{2+}$.

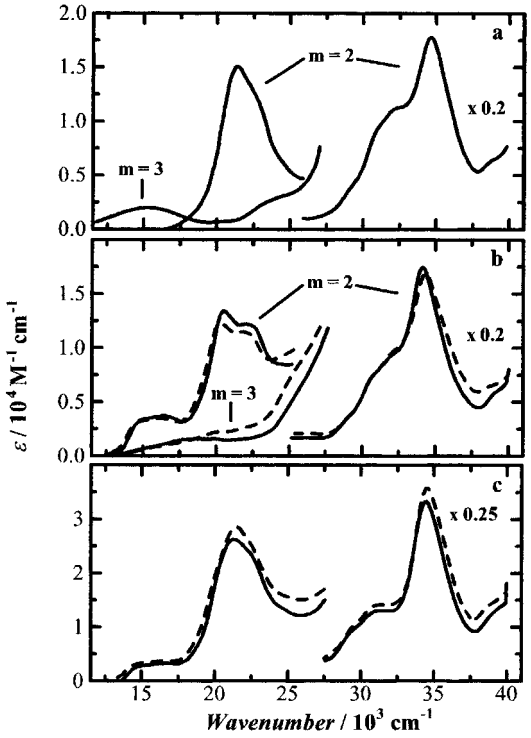


**Figure 2.** Absorption spectra of $[(dmb)_2Ru(L\text{-}C_5\text{-}L)]^{m+}$ (a), $[(L_\alpha)_2Os(L\text{-}C_5\text{-}L)]^{m+}$ (b), and $[(dmb)_2Ru(L\text{-}C_5\text{-}L)Os(L_\alpha)_2]^{4+}$ (c) in an AN solution containing 0.05 M of TEAP at room temperature: solid lines, $L_\alpha$ = bpy; dashed lines, $L_\alpha$ = dmb.

**Transient Absorption Spectra of Mixed-Valence Complexes.** Picosecond time-resolved spectra obtained after the excitation of $[(dmb)_2Ru^{II}(L\text{-}C_5\text{-}L)Os^{III}(bpy)_2]^{5+}$ are shown in Figure 4a. The TA spectrum observed at 20 ps after the excitation was similar to that of $[(dmb)_2Ru(L\text{-}C_5\text{-}L)]^{2+}$ (Figure 3b) except for the appearance of a broad band around 800 nm. The ($^3$CT)Ru excited state subsequently evolved to another intermediate, which showed an absorption peak at 515 nm and a broad band in the 600−700 nm region. The lifetime of the ($^3$CT)Ru state, which was 700 ns for $[(dmb)_2Ru^{II}(L\text{-}C_5\text{-}L)]^{2+}$,

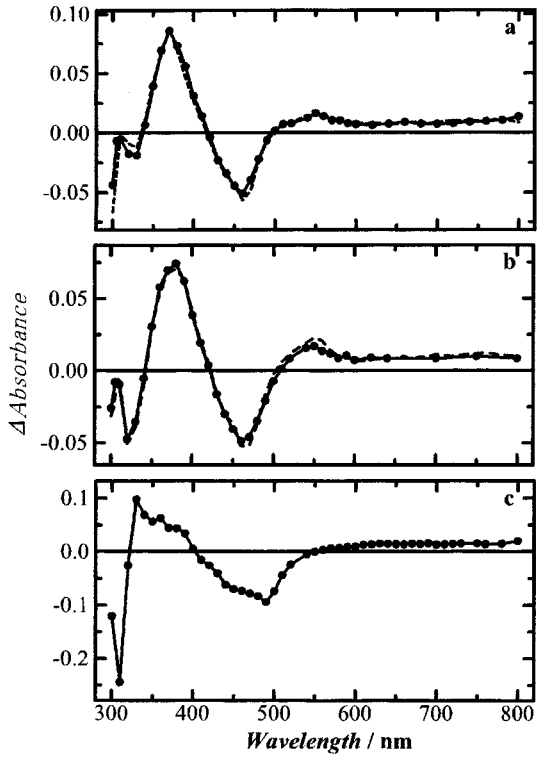


**Figure 3.** TA spectra upon excitation ($\lambda = 532$ nm) of $[(bpy)_2Ru(L\text{-}C_5\text{-}L)]^{2+}$ (a), $[(dmb)_2Ru(L\text{-}C_5\text{-}L)]^{2+}$ (b), and $[(bec)_2Ru(L\text{-}C_5\text{-}L)]^{2+}$ (c) in a BN solution at room temperature (solid lines) and 163 K (dashed lines).

was reduced to less than 100 ps in the MV complex. The resulting intermediate was assigned to a valence-isomer state (vide infra). Figure 4b shows the time evolution characteristic of the excited state (at 465 nm) and of the valence-isomer state (at 515 and 650 nm) from which the decay rate of ($^3$CT)Ru and BET rate were estimated. The isomer state decayed via BET within 6 ns. The broad absorption band around 800 nm decayed rapidly. While such a rapid decay was not observed for the Ru mononuclear or the Ru(II)−Ru(III) mixed-valence complexes, it was observed upon excitation of the Os(III) mononuclear complexes. Figure 5 shows the TA spectral changes following 532 nm excitation of $[(dmb)_2Os(L\text{-}C_4\text{-}L)]^{3+}$. Broad absorption bands appeared in 400−450 and 600−800 nm regions, and the LMCT band around 500−600 nm disappeared. The TA that remained up to 6000 ps at 460 nm is due to unoxidized mononuclear complex. The lifetime of this species was determined to be 10 ps from analysis of the decay profile of the TA at 750 nm.

Also for $[(bec)_2Ru^{II}(L\text{-}C_5\text{-}L)Ru^{III}(bpy)_2]^{5+}$, the decay kinetic was a biexponential. The TA spectra show that the initially formed ($^3$CT)Ru excited state of the $[(bec)_2Ru^{II}L]^{2+}$ moiety changed to another intermediate within a period of 1 ns. We identified this intermediate to be the valence-isomer state in the previous report.[6a] The lifetime of the excited state was short (1250 ps) compared to 600 ns of the mononuclear complex, $[(bec)_2Ru(L\text{-}C_5\text{-}L)]^{2+}$. The BET rates were determined from the biphasic change of negative absorption at 495 nm, which is due to the loss of MLCT absorption both in the $^3$CT excited state of the $[(bec)_2Ru^{II}L]$ moiety and valence isomer.

The decay rates of ($^3$CT)Ru ($k_{es}$) and the isomer state ($k_b$) are listed in Table 5. In a glassy BN solution at 113 K, the ($^3$CT)Ru excited state decayed with a rate of $k'_{es}$ and no TA due to the ET product was observed. For some of the MV compounds, $k'_{es}$ is collected in Table 5.

**Temperature Dependence of ET Rates and ET Yield.**

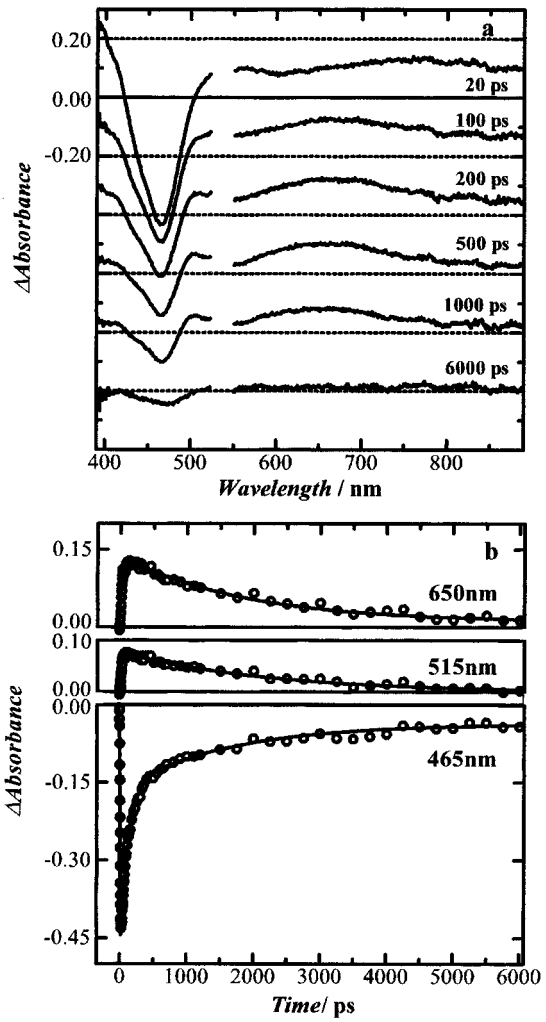


**Figure 4.** Picosecond time-resolved TA spectra for $[(dmb)_2Ru^{II}(L\text{-}C_5\text{-}L)Os^{III}(bpy)_2]^{5+}$ in a BN solution containing 0.1 M of TBAP at room temperature (a) and the time evolutions of the TA at 465, 515, and 650 nm (b). The solid lines in (b) were obtained using eq 7 (see text); $k_{es} = 9.7 \times 10^9$ s$^{-1}$, $k_b = 5.8 \times 10^8$ s$^{-1}$.

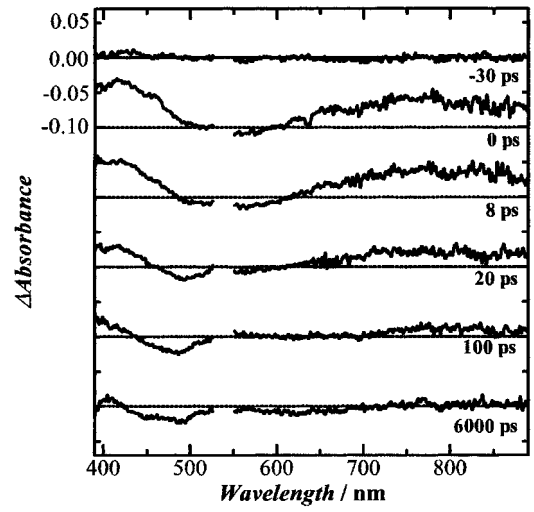


**Figure 5.** Picosecond time-resolved TA spectra for $[(dmb)_2Os(L\text{-}C_4\text{-}L)]^{3+}$ in a BN solution containing 0.1 M of TBAP at room temperature.

Figure 6a shows a plot of ln $k$ ($k$ stands for $k_{es}$, $k_{et}$, and $k_b$) vs $T^{-1}$ and the temperature dependence of ET yield, $\phi_{et}$, for the $[(dmb)_2Ru^{II}(L\text{-}C_5\text{-}L)Os^{III}(bpy)_2]^{5+}$ complex in BN. The plot shows a linear relationship and gives the activation energy and the frequency factor for the ET rates. ln $k$ for the other MV

**TABLE 5: ET Efficiency ($\phi_{et}$) and Rate Constants of Excited State Decay ($k_{es}$), Forward ET ($k_{et}$), and BET ($k_b$)[a]**

| compound | $k_{es}$ $10^9/s^{-1}$ | $k_{et}$ $10^9/s^{-1}$ | $k_{en}$[b] $10^9/s^{-1}$ | $\phi_{et}$ | $k_b$ $10^9/s^{-1}$ | $k'_{es}$[c] $10^9/s^{-1}$ |
|---|---|---|---|---|---|---|
| $[(dmb)_2Ru(L\text{-}C_3\text{-}L)Os(bpy)_2]^{5+}$ | $41 \pm 2.0$ | $5.0 \pm 0.4$ | $36 \pm 4$ | $0.15 \pm 0.1$ | $4.2 \pm 0.2$ | $30 \pm 4$ |
| $[(dmb)_2Ru(L\text{-}C_4\text{-}L)Os(bpy)_2]^{5+}$ | $15 \pm 1.0$ | $5.5 \pm 0.6$ | $9.5 \pm 0.4$ | $0.4 \pm 0.1$ | $1.4 \pm 0.1$ | $11.5 \pm 0.3$ |
| $[(dmb)_2Ru(L\text{-}C_4\text{-}L)Os(dmb)_2]^{5+}$ | $15 \pm 1.4$[d] | $5.6 \pm 0.6$[d] | $9.4 \pm 0.6$[d] | $0.35 \pm 0.1$[d] | $2.7 \pm 0.1$[d] | $10.6 \pm 1.7$[d] |
| $[(dmb)_2Ru(L\text{-}C_5\text{-}L)Os(bpy)_2]^{5+}$ | $9.7 \pm 0.8$ | $5.5 \pm 0.6$ | $4.2 \pm 0.6$ | $0.5 \pm 0.1$ | $0.58 \pm 0.09$ | |
| $[(dmb)_2Ru(L\text{-}C_5\text{-}L)Os(dmb)_2]^{5+}$ | $12.8 \pm 2.0$ | $5.1 \pm 0.5$ | $7.7 \pm 0.5$ | $0.4 \pm 0.1$ | $1.5 \pm 0.1$ | |
| $[(bec)_2Ru(L\text{-}C_3\text{-}L)Ru(bpy)_2]^{5+}$ | $3.5 \pm 0.1$ | | | | | |
| $[(bec)_2Ru(L\text{-}C_4\text{-}L)Ru(bpy)_2]^{5+}$ | $1.2 \pm 0.1$ | $0.3 \pm 0.02$ | $0.9 \pm 0.1$ | $0.25 \pm 0.1$ | $0.15 \pm 0.03$ | |
| $[(bec)_2Ru(L\text{-}C_5\text{-}L)Ru(bpy)_2]^{5+}$ | $0.82 \pm 0.03$ | $0.45 \pm 0.05$ | $0.43 \pm 0.04$ | $0.5 \pm 0.1$ | $0.12 \pm 0.04$ | |
| $[(bec)_2Ru(L\text{-}C_{10}\text{-}L)Ru(bpy)_2]^{5+}$ | 0.031[e] | 0.016[e] | 0.016[e] | $0.5 \pm 0.1$ | 0.018[e] | |

[a] In a BN solution containing 0.1 M of TBAP at 298 K. [b] $k_{en} = k_{es} - k_{et}$. [c] In a glassy BN solution containing 0.01 M of TBAP at 113 K. [d] In BN/AN mixture (9:1) containing 0.01 M of TBAP. [e] $\pm 0.001$.

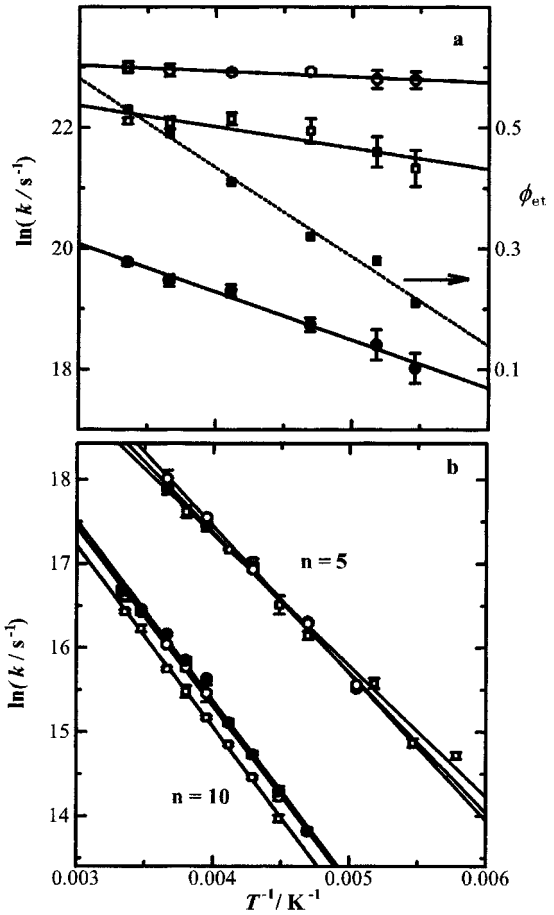


**Figure 6.** ln $k$ plotted against $T^{-1}$. $k$ defined as (a) the decay rate of the excited state, $k_{es}$ (○), the forward ET rate, $k_{et}$ (□), and the BET rate, $k_b$ (●), for $[(dmb)_2Ru^{II}(L\text{-}C_5\text{-}L)Os^{III}(bpy)_2]^{5+}$ in a BN solution containing 0.1 M of TBAP and (b) $k_b$ for $[(bec)_2Ru^{II}(L\text{-}C_n\text{-}L)Ru^{III}(bpy)_2]^{5+}$ ($n$ = 5 and 10) in a BN solution containing various concentrations of TBAP: 0.2 M (●), 0.01 M (○), and 0.002 M (□). Also shown in (a) is the temperature dependence of ET yield, $\phi_{et}$ (■).

compounds also shows a linear dependence on temperature. $E_a$ and $A$ values are summarized in Table 6.

**Variation of Back ET Rates with Ionic Strength.** Figure 6b shows the temperature dependence of BET rates, $k_b$, for $[(bec)_2Ru^{II}(L\text{-}C_n\text{-}L)Ru^{III}(bpy)_2]^{5+}$ ($n$ = 5, 10) in BN solutions containing various amount of tetra-*n*-butylammonium perchlorate (TBAP, 2−200 mM). Lines in the figure were obtained by least-squares fits to the data. For $n$ = 10, the BET rates decreased slightly with decreasing the salt concentration, whereas such an ion strength dependence was not observed for $n$ = 5 as seen in Figure 6b.

## Discussion

**On Redox Potentials of Mono- and Binuclear Complexes.** By comparing the first reduction potential of mononuclear complexes, it becomes clear that the reduction of ligand occurs in the order bec > bpy > L-$C_n$-L > dmb. The difference in LUMO energy between bec and L-$C_5$-L is ca. 450 mV, estimated as the difference in the first reduction potential between $[(dmb)_2M(L\text{-}C_5\text{-}L)]^{2+}$ and $[(bec)_2M(L\text{-}C_5\text{-}L)]^{2+}$. Differences between bpy and dmb can be calculated from the first reduction potential of their tris compounds, i.e., $[M(bpy)_3]^{2+}$ and $[M(dmb)_3]^{2+}$, which is ca. 180 mV. The difference (ca. 60 mV) in the first reduction potential between $[(bpy)_2M(L\text{-}C_5\text{-}L)]^{2+}$ and $[(dmb)_2M(L\text{-}C_5\text{-}L)]^{2+}$ cannot be ascribed to the energy gap between LUMO energy levels of bpy and dmb but to that between bpy and L-$C_5$-L.

As noted, the reduction potentials are shifted to less negative values on going from Ru(II) to Os(II). The origin of such an effect appears to be the increased $\sigma$-electron acceptability of M(II) as ruthenium(II) is replaced by osmium(II), while a d$\pi$−$\pi$* back-bonding between Os(II) and bpy-type ligands reduces the $\sigma$-electron population in metal d orbitals.[16]

Similar redox potentials of the metal-based oxidations in mono- and binuclear complexes, and also very weak IT bands for this family of complexes, indicate that they can be classified as class I MV compounds.[17]

**Energy Transfer in Ru(II)−Os(II) Systems.** It has been proposed that dipole−dipole interaction is predominant for slow energy transfer within donor−acceptor compounds containing heavy metal ions such as Ru(II)[18] and Os(II).[6b,19] The contribution of exchange interaction makes the rate to be much faster than that calculated assuming only a dipole−dipole interaction.[9,20,21]

The rates of excitation energy transfer, $k_{EN}$, from ($^3$CT)Ru to Os(II) moiety at 298 and 77 K are compared with those obtained by applying the Förster (Coulombic) approach, eq 5.[22] In this equation, the contribution to the rate constant comes from the dipole−dipole interaction between a donor and an acceptor (linked to each other in our system).

$$k_{EN} = \frac{9000 \ln 10\, \kappa^2 \phi_D}{128\pi^5 n^4 N \tau_D R_{DA}^6} \int F_D(\tilde{\nu})\, \epsilon_A(\tilde{\nu})^{-4}\, d\tilde{\nu} \qquad (5)$$

Here, $\tilde{\nu}$ is the wavenumber, $F_D(\tilde{\nu})$ is the spectral distribution of the emission normalized to unity, and $\epsilon_A(\tilde{\nu})$ is the molar extinction coefficient for the singlet−triplet absorption band of the acceptor. $k$ is the orientation factor (for random distributions of donor and acceptor assumed to be 1) and $\phi_D$ and $\tau_D$ are the quantum yield and lifetime of donor emission, respectively. $N$ is Avogadro's number and $n$ is the refractive index of solvent. The calculated values and the observed rates are given in Table

**TABLE 6: Electron Transfer Parameters Obtained by Analyzing The ET Rates[a]**

| | | forward ET | | | | | backward ET | | | | |
|---|---|---|---|---|---|---|---|---|---|---|---|
| compound | $\lambda_{out}^{298}$/eV | $\lambda_{in}$/eV | $\Delta G°$/eV | $H_{rp}$[b]/meV | $E_a$[c]/meV | $A$[c]/$10^{10}$ s$^{-1}$ | $\lambda_{in}$/eV | $\Delta G°$/eV | $H_{rp}$[b]/meV | $E_a$[c]/meV | $A$[c]/$10^{10}$ s$^{-1}$ |
| $[(dmb)_2Ru(L\text{-}C_3\text{-}L)Os(bpy)_2]^{5+}$ | 0.83 | 0.10 | −1.68 | **4.3** | 30[d] | 1.5[d] | <0.08 | −0.32 | **2.5** | 17 | 0.6 |
| $[(dmb)_2Ru(L\text{-}C_4\text{-}L)Os(bpy)_2]^{5+}$ | 0.89 | 0.10 | −1.68 | **3.0** | 41 | 2.0 | <0.08 | −0.32 | **1.9** | 30 | 0.4 |
| $[(dmb)_2Ru(L\text{-}C_5\text{-}L)Os(bpy)_2]^{5+}$ | 0.93 | 0.12 | −1.68 | **2.2** | 30 | 1.5 | 0.08 | −0.32 | **1.6** | 69 | 0.6 |
| $[(dmb)_2Ru(L\text{-}C_5\text{-}L)Os(dmb)_2]^{5+}$ | 0.90 | 0.09 | −1.58 | **2.0** | 43 | 2.3 | 0.11 | −0.42 | **1.6** | 27 | 0.4 |
| $[(bec)_2Ru(L\text{-}C_4\text{-}L)Ru(bpy)_2]^{5+}$ | 0.84 | 0.08 | −1.71 | **1.2**[e] | | | 0.10 | −0.19 | **2.0** | 123 | 2.5 |
| $[(bec)_2Ru(L\text{-}C_5\text{-}L)Ru(bpy)_2]^{5+}$ | 0.88 | 0.08 | −1.71 | **1.1**[e] | | | 0.10 | −0.19 | **1.6** | 144 | 2.7 |

[a] In a BN solution containing 0.1 M of TBAP (173K ≤ $T$ ≤ 298 K). [b] Uncertainty is less than 10%. [c] Estimated error is 10%. [d] In this system ($n$ = 3), estimated error is 30% due to a low ET yield. [e] Obtained only by method B (the $S$ value ($=\lambda_{in}/h\nu_M$) for forward ET is assumed to be the same as that for the radiative transition of ($^3$CT)Ru mononuclear).

3. The distance between transition dipoles ($R_{DA}$) in $[(dmb)_2Ru^{II}(L\text{-}C_n\text{-}L)Os^{II}(L_\alpha)_2]^{4+}$, $n$ = 3, 4, and 5, were assumed to be 10.5, 12, and 13 Å, respectively, which are obtained from molecular models assuming (i) an extended conformation of the methylene chains due to electrostatic repulsion between Ru(II) and Os(II) and (ii) a smaller value for $R_{DA}$ than the metal-to-metal distance. In the latter, we assumed that the interacting dipoles are centered between the (2-pyridyl)imidazole group and metal ion itself and along the bisector of N−M−N angle. Therefore, $R_{DA}$ is estimated to be shorter by ca. 2 Å than the metal-to-metal distance.

The observed rates are in good agreement with the calculated values (Table 3). Therefore, it seems reasonable to suggest that energy transfer in these series takes place via the Förster mechanism and that an exchange interaction does not play a major role.

There is a possibility that the intermetallic distance decreases as electrostatic repulsion is reduced by increasing ionic strength. However, the rates obtained are almost independent of TBAP salt concentration in the range of 0.002−0.2 M, within the experimental errors, which indicates that the conformation continues to be extended under these condition.

Although the energy transfer rate, $k_{EN}$, in Ru−Ru complexes showed somewhat strong temperature dependence,[9] in Ru−Os complexes it was fairly small; $k_{EN}$ decreased by 20−40% on going from 298 to 77 K (Table 3). The same phenomena have been observed in a rigid rodlike Ru−Os system.[7] The small temperature dependence of the energy transfer rates can be attributed to a considerable overlap between emission and absorption spectra of two moieties, which keeps the overlap integral almost constant even over a wide range of temperature. On the contrary, the overlap integral in $[(bec)_2Ru(L\text{-}C_5\text{-}L)Ru(bpy)_2]^{4+}$ is very sensitive to the position and shape of the donor emission spectrum as a consequence of temperature change, due to a poor spectral overlap. For example, the rate of energy transfer in $[(bec)_2Ru(L\text{-}C_n\text{-}L)Ru(bpy)_2]^{4+}$ decreased with increasing temperature at 110−170 K, where the highest energy emission bands of the donor moiety, $[Ru(bpy)_2]^{2+}$, are shifted to lower energy.[9] These results indicate that the distance between chromophores is kept almost constant in a wide temperature range or in different ionic strengths.

A small difference between observed and calculated rates probably arises because the actual $R_{DA}$ is slightly shorter than that obtained assuming the methylene chain is extended. Furthermore, the increasing length of the methylene chains reduces the electrostatic repulsion between the ionic centers, and the fraction of the extended form might be expected to decrease for the longer chain binuclears. There is also a considerably favorable entropy associated with more folded conformations. However, the fact that the observed rates in $Ru(II)(L\text{-}C_n\text{-}L)Os(II)$ approach the calculated ones indicates that the donor−acceptor distance is not so different from what has been assumed, at least in the cases where $n \leq 5$.

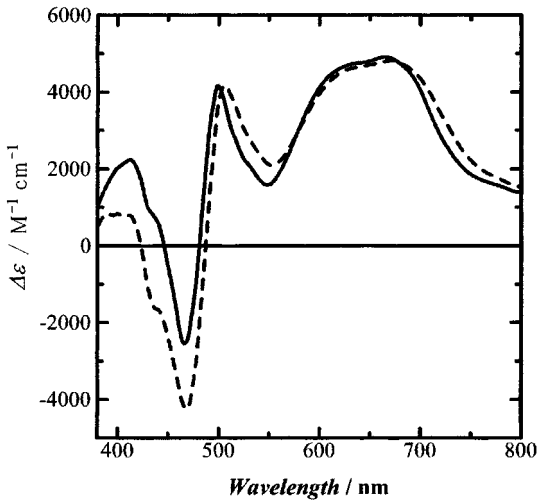


**Figure 7.** Simulated difference-absorption spectra for the formation of $[(dmb)_2Ru^{III}(L\text{-}C_5\text{-}L)Os^{II}(L_\alpha)_2]^{5+}$ from $[(dmb)_2Ru^{II}(L\text{-}C_5\text{-}L)Os^{III}(L_\alpha)_2]^{5+}$ using eq 6: solid line, $L_\alpha$ = bpy; dashed line, $L_\alpha$ = dmb.

**Picosecond Time-Resolved TA Spectra of Ru(II)−M(III).** *Identification of Intermediates.* Following the excitation of Ru(II)−M(III) complexes, a quenching process takes place via an ET mechanism giving the thermodynamically unstable Ru(III)−M(II) valence-isomer state. It subsequently converts to the stable isomer in the ground state via BET process (Figure 4a). This was confirmed by comparing the observed absorption spectra with the simulated absorption spectra for the Ru(III)−M(II) valence-isomer state (Figure 7). These spectra were obtained using eq 6, neglecting electronic interaction in absorption spectra

$$\Delta\epsilon = \epsilon_{Ru^{III}} - \epsilon_{Ru^{II}} + \epsilon_{M^{II}} - \epsilon_{M^{III}} \qquad (6)$$

where $\epsilon$'s are the molar extinction coefficients of Ru and M (Os or Ru) mononuclear complexes in each oxidation state, $[(L_\alpha)_2M(L\text{-}C_5\text{-}L)]^{2+/3+}$. In Figure 7, the absorption maximum at 510 and a broad band at 600−700 nm are specific to the Ru(III)−Os(II) state (for example: $\Delta\epsilon$ = 4700 M$^{-1}$ cm$^{-1}$ in $[(dmb)_2Ru^{III}(L\text{-}C_n\text{-}L)Os^{II}(bpy)_2]^{5+}$ at 650 nm, and −9600 M$^{-1}$ cm$^{-1}$ in $[(bec)_2Ru^{III}(L\text{-}C_n\text{-}L)Ru^{II}(bpy)_2]^{5+}$ at 490 nm[6a]). The TA spectrum at 500 ps in Figure 4a is very similar to that simulated except around 450 nm. Deviation around 450 nm is ascribed to the presence of a long-lifetime impurity, namely, ($^3$CT)Ru−Os(II) or Ru(II)−($^3$CT)Os of the unoxidized form.

*Forward and Backward ET Rates.* Schemes 1 and 2 illustrate the energy diagrams and photoinduced intramolecular processes in Ru−Os and Ru−Ru complexes, respectively. The energy level of the valence-isomer state was estimated from the redox potentials of the mononuclear complexes. In these schemes, $k_{et}$, $k_b$, and $k_{es}$ represent forward ET rate, back ET rate, and decay rate of excited state in the binuclear complex, respectively.

**SCHEME 1**

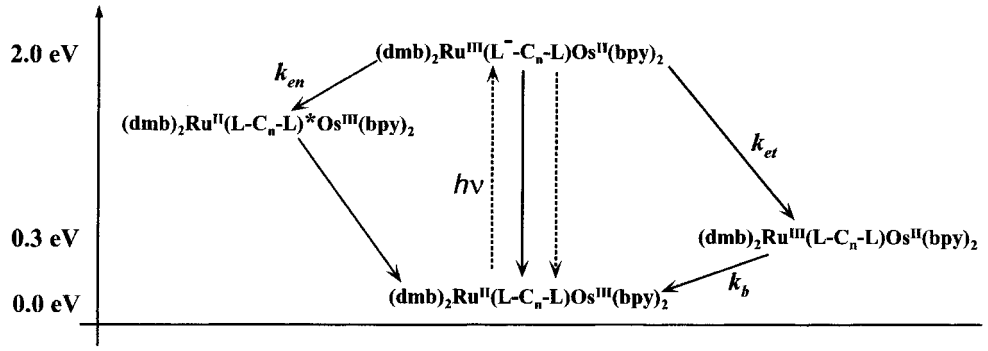


**SCHEME 2**

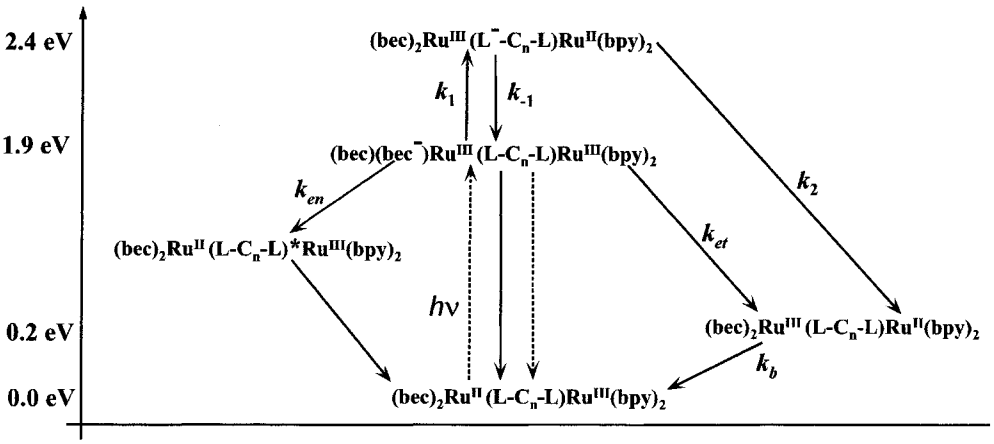


The decay of TA can be represented using a biexponential function as in eq 7.

$$A_t = A_1 \exp(-k_{es}t) + A_2 \exp(-k_b t) \quad (7)$$

The rate laws of the intermediates are given by eqs 8 and 9.

$$\frac{d[*Ru-M^{III}]}{dt} = -k_{es}[*Ru-M^{III}] \quad (8)$$

$$\frac{d[Ru^{III}-M^{II}]}{dt} = k_{et}[*Ru-M^{III}] - k_b[Ru^{III}-M^{II}] \quad (9)$$

By solving eqs 8 and 9, one obtains the following relationships, eqs 10 and 11.

$$A_1 = [*Ru-M^{III}]_0\left(\Delta\epsilon_{es} - \frac{\Delta\epsilon_{is}k_{et}}{k_{es}-k_b}\right) \quad (10)$$

$$A_2 = [*Ru-M^{III}]_0\left(\frac{\Delta\epsilon_{is}k_{et}}{k_{es}-k_b}\right) \quad (11)$$

In these equations, $[*Ru-M^{III}]_0$ is the initial concentration of *Ru−M(III), $\Delta\epsilon_{es}$ and $\Delta\epsilon_{is}$ are difference transient extinction coefficients of excited and valence-isomer states against the ground state, respectively. Thus, the ET rate and ET efficiency, $\phi_{et}$, can be determined from eqs 12 and 13, respectively.

$$k_{et} = (k_{es}-k_b)\left(\frac{A_2}{\Delta\epsilon_{is}}\right)\left(\frac{\Delta\epsilon_{es}}{A_1+A_2}\right) \quad (12)$$

$$\phi_{et} = k_{et}/k_{es} \quad (13)$$

In our actual calculation of $k_{et}$ and $\phi_{et}$, we used $A_2/\Delta\epsilon_{is}$ and $(A_1 + A_2)/\Delta\epsilon_{es}$ values obtained at different wavelengths for minimizing the calculation error (for example in Ru(II)−Os(III), 650 and 465 nm, respectively). The component with a very short lifetime observed in both Ru−Os MV complexes and $[(dmb)_2Os(L\text{-}C_4\text{-}L)]^{3+}$ (Figures 4 and 5) can be attributed to the decay of an LMCT excited state of the Os(III) moiety,[23] because $[(dmb)_2Os(L\text{-}C_4\text{-}L)]^{3+}$ shows an LMCT absorption band at the excitation wavelength (1600 $M^{-1}$ $cm^{-1}$, at 532 nm) and this band bleached over a wavelength range of 500−600 nm upon excitation. The TA that appeared around 400−450 and 650−900 nm are probably due to MLCT absorption bands of Os(II) and cation radical of the ligand, respectively. While the LMCT excited state can be formed by a direct excitation at 532 nm, it can be also produced from the ($^3$CT)Ru excited state via an energy transfer process. However, this state was not detected as an energy transfer product because of its very short lifetime (<15 ps) compared with the ($^3$CT)Ru excited state. In the analysis, using eq 7, the decay of the LMCT excited state was neglected because it was observable only during the excitation.

In $[(bec)_2Ru^{II}(L\text{-}C_5\text{-}L)Ru^{III}(bpy)_2]^{5+}$, the molar extinction coefficient of the LMCT band of Ru(III), $[(bpy)_2Ru^{III}(L\text{-}C_5\text{-}L)]^{3+}$ (430 $M^{-1}$ $cm^{-1}$ at 532 nm), is 10 times smaller than that of the donor, $[(bec)_2Ru^{II}(L\text{-}C_5\text{-}L)]^{2+}$ (4500 $M^{-1}$ $cm^{-1}$ at 532 nm). Thus, the excitation of Ru(III) center need not be considered.

The values of $k_{et}$ and $\phi_{et}$ are gathered in Table 5. For $[(dmb)_2Ru^{II}(L\text{-}C_n\text{-}L)Os^{III}(bpy)_2]^{5+}$, the $\phi_{et}$ is ca. 0.5 in $n = 5$ and decreases along with the decreasing $n$ value or temperature. The temperature dependence of $\Delta\epsilon_{is}$ at 650 nm for the Ru(III)−Os(II) isomer state was neglected because the shape of the broad MLCT band of the Os(II) moiety is not affected by temperature variation.

The fact that ET efficiencies are lower than unity indicates the occurrence of another process quenching the ($^3$CT)Ru excited

state, most probably an energy transfer producing the LMCT excited state of the Os(III) moiety. The rate of the competing process is shown as $k_{en}$ in Table 5. The decrease of $\phi_{et}$ with lowering temperature (Figure 6a) indicates that the competing process is activationless while the forward ET process has a small thermal barrier. This is confirmed by the results obtained in low-temperature glassy BN solution (at 113 K); the competing process preferably quenches the ($^3$CT)Ru excited state rather than the ET process, and the excited-state decay rate ($k'_{es}$) is similar to $k_{en}$ (Table 5). Therefore, the other quenching process in these systems, most likely, is a temperature-independent energy transfer from a ($^3$CT)Ru moiety to an Os(III) moiety.

In the system of $[(bec)_2Ru^{II}(L\text{-}C_n\text{-}L)Ru^{III}(bpy)_2]^{5+}$, ET efficiency was found to be 0.5 for $n = 5$, and by decreasing the donor−acceptor distance the ET efficiency decreased; 0.25 for $n = 4$. We were not able to observe BET in $[(bec)_2Ru^{II}(L\text{-}C_3\text{-}L)Ru^{III}(bpy)_2]^{5+}$, and thus the estimated ET efficiency is less than 0.1. Accordingly, $k_{et}$ could not be calculated in this system ($n = 3$). Concerning the small extent of ET efficiencies in this series of MV complexes, the speculated intramolecular energy transfer process becomes more favorable when the distance between donor and acceptor is shorter. The result is consistent with the fact that the energy transfer rate depends on the distance more strongly than the ET rate (see also Table 5).[24] A rapid BET process originated from the vibrationally excited states of valence isomer can also lower the efficiency.[5a] Such a low $\phi_{et}$ has been observed in strongly or intermediately coupled MV complexes ($H_{rp} > 10$ meV).[25] However, the rapid BET is unlikely to be significant in weakly coupled MV complexes such as those examined here (vide infra).

**Salt Effect on BET Rate of $[(bec)_2Ru^{II}(L\text{-}C_n\text{-}L)Ru^{III}(bpy)_2]^{5+}$ ($n = 5$, 10) and Flexibility of the Methylene Chain.** The use of longer methylene chains (for example, $n = 10$) allows close contact of donor and acceptor, which leads to a faster energy or ET process than expected.[9,26] Moreover, BET rates slightly increased with increasing salt concentration when $n = 10$. These results seem to be caused by shortening of the distance between two moieties as salt concentration increases (Figure 6b). The extent of ionic atmosphere determines the electrostatic repulsive forces between metal ions; the higher the ionic strength, the less the magnitude of repulsion between two ends of molecule. On the other hand, in the case where $n = 5$, the effect of ionic strength, if any, was less than the sensitivity of the measuring system, and salt concentration had relatively little effect on $E_a$ or $k_{et}$. Together with this fact, the good agreement between the observed values of energy transfer and calculated ones in $[(dmb)_2Ru^{II}(L\text{-}C_n\text{-}L)Os^{II}(L_\alpha)_2]^{4+}$ ($n = 3$, 4, 5) shows that the methylene chains have a nearly extended conformation in these binuclear complexes.

**Determination of $H_{rp}$ for Forward and Backward ET Processes.** The observed ET rates were analyzed using nonadiabatic ET theory represented by eq 14[27]

$$k = \frac{2[H_{rp}]^2}{h}\sqrt{\frac{\pi^3}{\lambda_{out}k_BT}}\sum\frac{e^{-S}S^m}{m!} \times \exp\left(-\frac{(\Delta G^\circ + \lambda_{out} + mh\nu)^2}{4\lambda_{out}k_BT}\right) \quad (14)$$

where $H_{rp}$, $\Delta G^\circ$, $h\nu$, and $S$ are electronic interaction matrix element of initial and final states, the free energy gap, the energy of the vibrational quantum for a medium-frequency accepting mode, and the electron−vibration coupling constant of the vibrational mode, respectively. The solvent reorganization energy, $\lambda_{out}$, is given by eq 15 using the two spheres model in a dielectric continuum[27]

$$\lambda_{out} = \frac{\Delta e^2}{4\pi\epsilon_0}\left(\frac{1}{\epsilon_{op}} - \frac{1}{\epsilon_s}\right)\left(\frac{1}{2r_D} + \frac{1}{2r_A} - \frac{1}{R'_{DA}}\right) \quad (15)$$

where donor and acceptor are considered as spheres with radii of $r_D$ and $r_A$ separated by a distance of $R'_{DA}$. $\epsilon_{op}$ and $\epsilon_s$ are the optical and static dielectric constants for the solvent. $\Delta e$ is the charge transferred, and $\epsilon_0$ is the permittivity of vacuum. Since the donor or acceptor moieties are not perfect spheres, their radii are difficult to be defined. We considered them as spheres whose van der Waals volumes are equivalent to that of the model complexes, $[(L_\alpha)_2M(mpbim)]^{2+}$. Then, $\lambda_{out}$ was calculated using radii of the model complexes and metal-to-metal distance. The radii used in the calculation of $\lambda_{out}$ are 4.9, 5.1, and 5.5 Å for $L_\alpha$ = bpy, dmb, and bec, respectively.

Using the above parameters and $R'_{DA} = 15$ Å (metal-to-metal distance, for $n = 5$), $\epsilon_{op} = 1.91$, and $\epsilon_s = 24.8$ for BN, $\lambda_{out}$ for $[(dmb)_2Ru^{II}(L\text{-}C_5\text{-}L)Os^{III}(bpy)_2]^{5+}$, $[(dmb)_2Ru^{II}(L\text{-}C_5\text{-}L)Os^{III}(dmb)_2]^{5+}$, and $[(bec)_2Ru^{II}(L\text{-}C_5\text{-}L)Ru^{III}(bpy)_2]^{5+}$ are calculated to be 0.93, 0.90, and 0.88 eV, respectively.

For the forward ET where the electron transfer originates from a ligand anion radical to the M(III) ion, a medium-frequency vibration mode of the ligand anion radical in the ($^3$CT)Ru state is considered to dominate the Franck−Condon factor, particularly in the inverted region.[28] This is the case for the radiative transition of ($^3$CT)Ru excited states. In the latter, the medium-frequency vibration and its $S$ value can be determined from the analysis of the CT emission spectra using eq 16 assuming one frequency mode of vibration involved in the emission.[29]

$$I_M(\tilde{\nu}) = \left(\frac{\tilde{\nu}}{\tilde{\nu}_{0-0}}\right)^3\Sigma\exp(-S_M)\frac{S_M^{n_M}}{n_M!}\sqrt{\frac{4\ln 2}{\pi\Delta\tilde{\nu}_{1/2}{}^2}} \times \exp\left(-\frac{4\ln 2\,(\tilde{\nu} - \tilde{\nu}_{0-0} + n_M\tilde{\nu}_M)^2}{\Delta\tilde{\nu}_{1/2}{}^2}\right) \quad (16)$$

In this equation $I_M(\tilde{\nu})$ is the emitted intensity at energy $\tilde{\nu}$, $\tilde{\nu}_{0-0}$ is the emission energy of the 0−0 transition, and $\Delta\tilde{\nu}_{1/2}$ is the full width at half-maximum (fwhm) for each transition band. Fitting to the emission spectra of the mononuclear complexes gave the parameters (for $[(dmb)_2Ru(L\text{-}C_5\text{-}L)](ClO_4)_2$, $\tilde{\nu}_{0-0} = 16\,000$, $\tilde{\nu}_M = 1300$, $\Delta\tilde{\nu}_{1/2} = 850$ cm$^{-1}$, and $S_M = 0.74$; for $[(bec)_2Ru(L\text{-}C_5\text{-}L)](ClO_4)_2$, $\tilde{\nu}_{0-0} = 15\,400$, $\tilde{\nu}_M = 1350$, $\Delta\tilde{\nu}_{1/2} = 800$ cm$^{-1}$, and $S_M = 0.48$ both in BN at 77 K). Then, the averaged frequency (1300 cm$^{-1}$) has been used for the determination of $H_{rp}$. On the other hand, the vibrational modes that must be considered in the BET process are those of the metal−nitrogen bond. Since a typical frequency for those vibrations is 400−600 cm$^{-1}$, we used 500 cm$^{-1}$ in the calculation of BET rates.

Next unknown parameters, $H_{rp}$ and $S$ were determined by the following two methods. Method A: the $H_{rp}$ and $S$ are simultaneously determined by fitting the temperature dependence of the forward and backward ET rates to eq 14.[30] In this analysis, the temperature dependence of $\lambda_{out}$ was considered using eq 17,

$$\lambda_{out}(T) = \lambda_{out}{}^{298}\,(0.822 + 1.14 \times 10^{-3}T - 1.82 \times 10^{-6}T^2) \quad (17)$$

where $\lambda_{out}{}^{298}$ is the calculated outer-sphere (solvent) reorganization energy in BN at room temperature ($173 < T \leq 298$). The contribution of intramolecular reorganization energy, $\lambda_{in}$,was estimated to be $\leq$0.12 eV for these electron transfers.

Method B: the $S$ value for the forward ET was assumed to be the same as that for the radiative transition of the ($^3$CT)Ru excited state, which was determined by analyzing the emission spectrum (eq 16). The observed ET rates were well reproduced by the latter method, giving exactly the same parameters obtained by method A (for the forward ET, see Table 6).

Two possible ET processes are proposed for the forward ET in $[(bec)_2Ru^{II}(L\text{-}C_n\text{-}L)Ru^{III}(bpy)_2]^{5+}$: a direct ET from bec to Ru(III) or a two-step ET involving the $[(bec)_2Ru(L^-)]$ state.[8] However, the two-step ET mechanism is ruled out by the following discussion in the framework of Scheme 2. The difference in energy of remote (R, $[(bec)(bec^-)Ru^{III}L]$) and adjacent (A, $[(bec)(bec)Ru^{III}L^-]$) states, $\Delta E$, is approximated to be the difference between the first reduction potentials in $[(bec)_2Ru(L\text{-}C_5\text{-}L)]^{2+}$ and $[(dmb)_2Ru(L\text{-}C_5\text{-}L)]^{2+}$ (0.45 V). Applying a steady-state approximation for the adjacent MLCT state concentration, [A], the time dependence of the remote MLCT state concentration, [R], is given by eq 18.

$$-\frac{d[R]}{dt} = \frac{k_1 k_2}{k_{-1} k_2}[R] = k_{obs}[R] \qquad (18)$$

When $k_{-1} \gg k_2$, the R and the A states are in equilibrium and MLCT population's ratio, $[A]/[R] = \exp(-\Delta E/RT)$, is estimated to be $2.5 \times 10^{-8}$ ($=k_1/k_{-1}$) from $\Delta E$. The value of $3.2 \times 10^{16}$ $s^{-1}$ calculated for $k_2$ to reproduce the observed rate in AN ($8 \times 10^8$ $s^{-1}$) is considerably larger than an optimum ET rate ($<10^{13}$ $s^{-1}$). On the other hand, $k_{obs}$ equals $k_1$ when $k_{-1} \ll k_2$. This and the ratio of $k_1/k_{-1}$ also give an unusual relationship, $k_2 \gg 3.2 \times 10^{16}$. Consequently, the possible ET process must be a direct ET from the remote MLCT state (Ru-bec$^{\bullet -}$) to the acceptor orbital of $Ru^{III}$-d$\pi$.

It is of great interest that the forward ET rates in the Ru(II)−Os(III) series are almost independent of the number of methylene groups ($n$), while the BET rates depend on $n$. This can be explained in terms of the distance dependence of $\lambda_{out}$ and $H_{rp}$. $\lambda_{out}$ increases along with distance (eq 15), while $H_{rp}$ decreases exponentially ($H_{rp}^2 \propto \exp(-\beta R'_{DA})$.) In the normal region, both the decreasing $H_{rp}$ and increasing $\lambda_{out}$ simply reduce ET rates. This is the case for BET rates. Meanwhile, the exponential term in eq 14 increases with increasing $\lambda_{out}$ in the inverted region, and therefore it cancels the effect of decreasing $H_{rp}$. Consequently, the ET rates depend very weakly on distance when the distance is relatively short.[31] This is probably the reason for the distance independence of forward ET rates.

The following features in the obtained parameters are of interest: (i) the $H_{rp}$ value for forward ET in $[(dmb)_2Ru^{II}(L\text{-}C_n\text{-}L)Os^{III}(L_\alpha)_2]^{5+}$ is nearly two times larger than that in $[(bec)_2Ru^{II}(L\text{-}C_n\text{-}L)Ru^{III}(bpy)_2]^{5+}$, while those for BET rates are equal. (ii) In $[(bec)_2Ru^{II}(L\text{-}C_n\text{-}L)Ru^{III}(bpy)_2]^{5+}$ the $H_{rp}$ value for BET is larger than that for forward ET, while in the case of $[(dmb)_2Ru^{II}(L\text{-}C_n\text{-}L)Os^{III}(L_\alpha)_2]^{5+}$ it is reversed. (iii) The similarity in $H_{rp}$ of BET in two types of binuclear complexes indicated that there is no measurable difference in the electronic interaction of Ru(II)−Ru(III) homobinuclear and Ru(II)−Os(III) heterobinuclears arising from a variation of metallic center (from Ru to Os). Features i and ii suggest that the $H_{rp}$ values appear to be correlated with the location of the excited electron. Thus in $[(bec)_2Ru^{II}(L\text{-}C_n\text{-}L)Ru^{III}(bpy)_2]^{5+}$, through-bond distance between electron donor on one side and electron acceptor on the other side of the binuclear complex is longer than that of $[(dmb)_2Ru^{II}(L\text{-}C_n\text{-}L)Os^{III}(L_\alpha)_2]^{5+}$ where the excited electron is dominantly localized on the bridging ligand. The difference in $H_{rp}$ between $[(bec)_2Ru^{II}(L\text{-}C_n\text{-}L)Ru^{III}(bpy)_2]^{5+}$ and $[(dmb)_2Ru^{II}(L\text{-}C_n\text{-}L)Os^{III}(L_\alpha)_2]^{5+}$ is ascribed to the distance as a consequence of the different localization of the excited electron.

On the contrary, the BET process involves electronic interaction between the d$\pi$ orbitals of metallic centers. Ignoring the differences in overlap integral between $\pi^*$(L)−d$\pi$(M) and d$\pi$(M)−d$\pi$(M), the increasing order of $H_{rp}$ is anticipated to agree with the decreasing order of the distance between interacting orbitals, $\pi^*$(bec)-d$\pi$(M) >, d$\pi$(M)−d$\pi$(M) >, $\pi^*$(L)−d$\pi$(M). This was found to be the case.

The $H_{rp}$ values in Table 6 indicate that the difference in $H_{rp}$ is not a major origin for the large difference between the forward ET rates of Ru(II)−Ru(III) and Ru(II)−Os(III) complexes. The forward ET rates in Ru(II)−Os(III) compounds are faster than those in Ru(II)−Ru(III) compounds by a factor of 12 where $n = 5$ and 18 where $n = 4$, obtained from the ratio of the forward ET rates in Table 5. From the resulting $H_{rp}$ values in Table 6, it turns out that approximately 30% of these factors are due to the difference in the electronic interaction, that is $[H_{rp}(Ru-Os)/H_{rp}(Ru-Ru)]^2/[k_{et}(Ru-Os)/k_{et}(Ru-Ru)] \sim 0.3$, and the other 70% can be attributed to the difference in other terms including $S$ (or $\lambda_{in}$) and $\lambda_{out}$ in eq 14. The small values of $H_{rp}$ are inconsistent with the occurrence of a rapid BET originating from vibrationally excited states of the valence isomer.[25]

## Conclusions

The effect of the extent of electronic interaction on the photoinduced intramolecular ET processes has been investigated. Our results enabled us to conclude that

(1) In the series investigated in this work, two metallic donor−acceptor centers are linked to each other with a 1,$n$-bis[2-(2-pyridyl)-1-benzimidazolyl]alkane ($n = 3, 4, 5$), where due to the electrostatic repulsion the conformation is extended into a nearly linear structure.

(2) With the $[(bec)_2RuL]^{2+}$ moiety as the electron donor in which the excited electron locates on the remote ligand(s), the $H_{rp}$ value decreases by half compared to those binuclear compounds with $[(dmb)_2RuL]^{2+}$ as donor in which the location of the excited electron is on the bridging ligand (L). Thus, for both types of binuclear compounds the difference in $H_{rp}$ is just related to the distance between a donor orbital and an acceptor one.

(3) The ET efficiency ($\phi_{et} \leq 0.5 \pm 0.1$) decreases along with the decreasing number of methylene groups or temperature, indicating the existence of another process quenching the ($^3$CT)-Ru excited state.

**Acknowledgment.** The authors acknowledge Prof. Y. Arakawa for his help in obtaining ESI-MS spectra. K.N. and T.O. gratefully acknowledges financial support for a Grant-in-Aid for Scientific Research (No. 06640654) and Priority-Area-Research "Photoreaction Dynamics" (No. 06239101), respectively, from the Ministry of Education, Science, Culture and Sports of Japan (MONBUSHO). B.G. is also thankful for a graduate scholarship awarded to him by MONBUSHO.

## References and Notes

(1) (a) Creutz, C. *Prog. Inorg. Chem.* **1983**, *30*, 1. (b) Hush, N. S. *Coord. Chem. Rev.* **1985**, *64*, 135.

(2) Hush, N. S. *Prog. Inorg. Chem.* **1967**, *8*, 391.

(3) McManis, G. E.; Nielson, R. M.; Gochev, A.; Weaver, M. J. *J. Am. Chem. Soc.* **1989**, *111*, 5533.

(4) Swaddle T. W. *Inorg. Chem.* **1990**, *29*, 5017.

(5) (a) Arnett, D. C.; Vohringer, P.; Scherer, N. F. *J. Am. Chem. Soc.* **1995**, *117*, 12262. (b) Tominaga, K.; Kliner, D. A. V.; Johnson, A. E.; Levinger, N. E.; Barbara, P. F. *J. Chem. Phys.* **1993**, *98*, 1228.

(6) (a) Nozaki, K.; Ohno, T. *Coord. Chem. Rev.* **1994**, *132*, 215. (b) De Cola, L.; Balzani, V.; Barigelletti, F.; Flamigni, L.; Belser, P.; Zelewsky, A. V.; Frank. M.; Vogtle, F. *Inorg. Chem.* **1993**, *32*, 5228. (c) Curtis, J. C.; Bernstein, J. S.; Meyer, T. J. *Inorg. Chem.* **1985**, *24*, 385. (d) Creutz, C.; Kroger, P.; Matsubara, T.; Netzel, T. L.; Sutin, N. *J. Am. Chem. Soc.* **1979**, *101*, 5442.

(7) Balzani, V.; Barigelletti, F.; Belser, P.; Bernhard, S.; De Cola, L.; Flamigni, L. *J. Phys. Chem.* **1996**, *100*, 16786.

(8) (a) Cooley, L. F.; Headford, C. E. L.; Elliott, C. M.; Kelley, D. F. *J. Am. Chem. Soc.* **1988**, *110*, 6673. (b) Cooley, L. F.; Larson, S. L.; Elliott, C. M.; Kelley, D. F. *J. Phys. Chem.* **1991**, *95*, 10694.

(9) Yoshimura, A.; Nozaki, K.; Ikeda, N.; Ohno, T. *Bull. Chem. Soc. Jpn.* **1996**, *69*, 2791.

(10) Arakawa, R.; Matuo, T.; Ito, H.; Hatakuse, I.; Nozaki, K.; Ohno, T.; Haga, M. *Org. Mass Spectrom.* **1994**, *29*, 289.

(11) Ohno, T.; Nozaki, K.; Haga, M. *Inorg. Chem.* **1992**, *31*, 548.

(12) Yoshimura, A.; Nozaki, K.; Ikeda, N.; Ohno, T. *J. Phys. Chem.* **1996**, *100*, 1630.

(13) Ohno, T.; Yoshimura, A.; Mataga, N. *J. Phys. Chem.* **1990**, *94*, 4871.

(14) Nakamura, K. *Bull. Chem. Soc. Jpn.* **1982**, *55*, 1639.

(15) (a) Ohsawa, Y.; DeArmond, M. K.; Hanck, K. W.; Morris, D. E.; Whitten, D. G.; Neveux, P. E., Jr. *J. Am. Chem. Soc.* **1983**, *105*, 6522. (b) DeArmond, M. K.; Carlin, C. M. *Coord. Chem. Rev.* **1981**, *36*, 325.

(16) Magnuson, R. H.; Taube, H. *J. Am. Chem. Soc.* **1975**, *97*, 5129.

(17) (a) Robin, M. B.; Day, P. *Adv. Inorg. Chem. Radiochem.* **1967**, *10*, 247. (b) Balzani, V.; Juris, A.; Venturi, M.; Campagna, S.; Serroni, S. *Chem. Rev. (Washington, D.C.)* **1996**, *96*, 759 and references therein.

(18) Schmehl, R. H.; Auerbach, R. A,; Wacholtz, W. F. *J. Phys. Chem.* **1988**, *92*, 6202.

(19) Furue, M.; Yoshidzumi, T.; Kinoshita, S.; Kushida, T.; Nozakura, S.; Kamachi, M. *Bull. Chem. Soc. Jpn.* **1991**, *64*, 1632.

(20) Ryu, C. K.; Schmehl, R. H. *J. Phys. Chem.* **1989**, *93*, 7961.

(21) Beley, M.; Chodorowski, S.; Collin, J.-P.; Sauvage, J.-P.; Flamigni, L.; Barigelletti, F. *Inorg. Chem.* **1994**, *33*, 2543

(22) Förster, Th. H. *Discuss. Faraday Soc.* **1959**, *27*, 7.

(23) Bergkamp, M. A.; Gutlich, P.; Netzel, T. L.; Sutin, N. *J. Phys. Chem.* **1983**, *87*, 3877.

(24) Closs, G. L.; Johnson, M. D.; Miller, J. R.; Piotrowiak, P. *J. Am. Chem. Soc.* **1989**, *111*, 3751.

(25) Nozaki, K.; Gholamkhass, B.; Ohno, T. To be submitted.

(26) Larson, S. L.; Elliott, C. M.; Kelley, D. F. *Inorg. Chem.* **1996**, *35*, 2070.

(27) Marcus, R. A.; Sutin, N. *Biochim. Biophys. Acta* **1985**, *811*, 265.

(28) For example: (a) Hager, G. D.; Crosby, G. A. *J. Am. Chem. Soc.* **1975**, *97*, 7031. (b) Dallinger, R. F.; Woodruff, W. H. *J. Am. Chem. Soc.* **1979**, *101*, 4391. (c) Clark. R. J. H.; Turtle, P. C.; Strommen, D. P.; Streusand, B.; Kincaid, J.; Nakamoto, K. *Inorg. Chem.* **1977**, *16*, 84.

(29) Caspar, J. V.; Westmoreland, T. D.; Allen, G. H.; Bradley, P. G.; Meyer, T. J.; Woodruff, W. H. *J. Am. Chem. Soc.* **1984**, *106*, 3492.

(30) To calculate these parameters, several assumptions have been made: (a) the same temperature dependence of dielectric constant ($\epsilon_s$) of BN as that for AN ($d\epsilon_s/dT = 0.215$ D/K (Liu, J.-Y.; Bolton, J. R. *J. Phys. Chem.* **1992**, *96*, 1718); (b) temperature independence of $H_{rp}$ and $\Delta G°$. Also temperature dependence of refractive index of BN considered as $dn/dT = 0.000\,43\ K^{-1}$ (Riddick, J. A.; Bunger, W. B.; Sakano, T. K. *Organic Solvents*, 4th ed.; Wiley: New York, 1986; Vol. 2, p 587).

(31) Tachiya, M.; Murata, S. *J. Phys. Chem.* **1992**, *26*, 8441.